JOURNAL OF
biomaterials
applications

Original Article

Journal of Biomaterials Applications
0(0) 1–13

DOI: 10.1177/0885328216633374
jba.sagepub.com
SAGE

Investigation of the *in vitro* photocatalytic antibacterial activity of nanocrystalline TiO_2 and coupled TiO_2/Ag containing copolymer on the surface of medical grade titanium

Ágnes Györgyey[1], László Janovák[2], András Ádám[3], Judit Kopniczky[4], Krisztián L Tóth[5], Ágota Deák[2], Ivan Panayotov[6], Frédéric Cuisinier[6], Imre Dékány[7] and Kinga Turzó[3]

Abstract

Antibacterial surfaces have been in the focus of research for years, driven by an unmet clinical need to manage an increasing incidence of implant-associated infections. The use of silver has become a topic of interest because of its proven broad-spectrum antibacterial activity and track record as a coating agent of soft tissue implants and catheters. However, for the time being, the translation of these technological achievements for the improvement of the antibacterial property of hard tissue titanium (Ti) implants remains unsolved. In our study, we focused on the investigation of the photocatalysis mediated antibacterial activity of silver (Ag), and Ti nanoparticles instead of their pharmacological effects. We found that the photosensitisation of commercially pure titanium discs by coating them with an acrylate-based copolymer that embeds coupled Ag/Ti nanoparticles can initiate the photocatalytic decomposition of adsorbed *S. salivarius* after the irradiation with an ordinary visible light source. The clinical isolate of *S. salivarius* was characterised with MALDI-TOF mass spectrometer, while the multiplication of the bacteria on the surface of the discs was followed-up by MTT assay. Concerning practical relevance, the infected implant surfaces can be made accessible and irradiated by dental curing units with LED and plasma arc light sources, our research suggests that photocatalytic copolymer coating films may offer a promising solution for the improvement of the antibacterial properties of dental implants.

Keywords

Titanium, photosensitisation, nanoparticle, antibacterial, silver, dental implant

Introduction

Dental implants today are increasingly becoming the preferred method to replace missing teeth. Due to their biocompatibility and high clinical success rate titanium dental implant based restorations are indeed very good choices for healthy patients.[1] Implant failure is mainly caused by inflammatory processes affecting the soft and hard tissues. Peri-implant mucositis is defined as a reversible inflammation of the peri-implant soft tissue, which can turn into irreversible peri-implantitis, when the bone is also affected.[2]

During the past 10 years, the incidence of peri-implant infections increased dramatically, especially in

[1]Department of Prosthodontics, Faculty of Dentistry, University of Szeged, Hungary
[2]Department of Physical Chemistry and Material Sciences, Faculty of Science and Informatics, University of Szeged, Hungary
[3]Department of Oral Biology and Experimental Dental Research, Faculty of Dentistry, University of Szeged, Hungary
[4]Department of Optics and Quantum Electronics, Faculty of Science and Informatics, University of Szeged, Hungary
[5]NanoTi Limited, Birmingham Research Park, UK
[6]Laboratoire Biosanté et Nanoscience, UFR Odontologie, University of Montpellier I, France
[7]MTA-SZTE Supramolecular and Nanostructured Materials Research Group, Faculty of Medicine, University of Szeged, Hungary

Corresponding author:
Ágnes Györgyey, Department of Prosthodontics, Faculty of Dentistry, University of Szeged, 6720 Szeged, Tisza Lajos krt. 64, Hungary.
Email: gyorgyey.agnes@gmail.com

the case of dental implants.[3,4] Several methods have been proposed for the treatment of peri-implantitis, however the issue still remains unsolved. The recent therapeutic approaches are mostly focusing on the removal of the contaminating agent from the implant surface. Conservative therapy has only been found effective in the treatment of peri-mucositis. When peri-implantitis emerges resective or regenerative surgical therapy becomes necessary. The aim of such surgical interventions is cleaning of the surface of the implants, while avoiding the mechanical destruction of the TiO_2 layer of the implant and the surrounding tissue, while also preventing the reattachment of pathogenic bacteria. Currently, there are no treatment methods available that could fulfil these requirements. Effective mechanical debridement causes irreversible damage to the surface of an implant. The adjuvant systemic or local antibacterial therapy cannot remove residual bacteria from the surface and cannot prevent the recurrence of the infection. Furthermore, the overuse of antibiotics during the last four decades has led to the emergence of new antibiotic resistant bacteria strains that aggravates the complications associated with peri-implant infections.[5] Removal of an infected implant is always accompanied by the destruction of the surrounding tissues that may entail severe complications, like bone loss, trauma of the adjacent teeth, fracture of the crestal bone or sinus exposure; therefore, it is always to be the last therapeutic choice.[6]

Antibacterial surfaces have been in the focus of research for years as potential alternatives of antibiotics to prevent the progression of peri-implant infections.[7] However, the scientific achievements have not been reduced to clinical practice so far.[8] Silver has gained a great deal of interest either as a doping or as a coating agent of titanium implants in various forms because of its proven broad-spectrum antibacterial activity.[9] The main limitation of the clinical application of silver containing implants is the unpredictable host tissue response to the high local concentration of silver on the surface of a bone substitute. Furthermore, little is known about the tissue distribution and the cellular uptake of silver, while silver ions can dissolve and silver nanoparticles can release from the surface of the indwelling implants.[10] Hence, in spite of the unquestionable antibacterial effect of silver containing surfaces it still requires extensive research to map the risks of potential side-effects associated with the pharmacological behaviour of silver.

On the other hand, silver nanoparticles exhibit unique photocatalytic properties that are already widely utilised in the semiconductor industry to improve the efficiency of TiO_2 in photocatalytic applications.[11] This feature may harbour untapped potential that might be exploited in the surface treatment of titanium dental implants.[12,13] Titanium dioxide is typically an *n*-type semiconductor due to oxygen deficiency and it is the most widely investigated photocatalyst because of its high photoactivity, low toxicity, good chemical and thermal stability.[14] In photocatalysis, light of energy greater than the band gap of the semiconductor, excites an electron from the valance band to the conduction band.[15] The excitation of an electron to the conduction band generates a positive hole in the valance band. Charge carriers (positive holes and electrons) can migrate to the catalyst surface and initiate redox reactions through the oxidation of adsorbed H_2O producing reactive oxidising species (hydroxide, superoxide radicals, etc.), which finally can lead to the photocatalytic degradation of the absorbed organic compounds, such as pyrogens and bacteria.[16] Various strategies have been adopted for enhancing the photocatalytic efficiency of TiO_2, including silver deposition that may have great future relevance in the surface modification of titanium dental implants.

Concerning potential dental applications, our hypothesis was that the photocatalytic activity of TiO_2 nanoparticles might be successfully utilised in the treatment of peri-implant infections in order to avoid the detrimental effect of mechanical decontamination of the surface of implants. From practical view, when peri-implantitis is diagnosed, the affected part of the implant is unfolded for surgical debridement, irradiation of the implant surface becomes possible. The irradiation induced accelerated release of reactive oxygen species may decompose the early-diagnosed biofilm on the surface of the dental implants and may render vigorous mechanical decontamination unnecessary.

The aim of the present work was to develop a novel copolymer that is supplemented with either TiO_2 or with coupled TiO_2/Ag photocatalysts and investigate their antibacterial activity in in vitro experimental setting. As a model organism *Streptococcus salivarius* was used in our experiments, which may be a first coloniser in titanium dental implant associated infections.[17]

Materials and methods

Preparation of titanium disc samples

For the experiments 1.5 mm thick 9 mm diameter discs were cut from commercially pure (CP4) titanium rods (Daido Steel, Japan®) and they were subjected to sand-blasting with aluminium oxide of 150 µm grain size (FINO, Germany) and, subsequently, to acid etching with nitric acid (Reanal, Hungary). Before further processing the samples were cleaned ultrasonically in acetone then 70% ethanol for 15 min and finally rinsed in ultrapure water. Then the titanium discs were coated with polymer-based photocatalytic films. The experimental groups are shown in Table 1.

Table 1. Experimental groups. Dark set comprises the number of samples that were stored in dark, while light set comprises the number of samples that were subjected to UV-Vis irradiation in each experimental group.

Surface types	Group	Dark set	Light set
Sandblasted and acid-etched surface	(A)	$n=16$	$n=16$
p(EA-co-MMA) copolymer	(B)	$n=16$	$n=16$
60 wt% TiO_2: 40 wt% copolymer	(C)	$n=16$	$n=16$
60 wt% DS-TiO_2: 40 wt% copolymer	(D)	$n=16$	$n=16$
60 wt% Ag-TiO_2: 40 wt% copolymer	(E)	$n=16$	$n=16$
60 wt% Ag-DS/TiO_2: 40 wt% copolymer	(F)	$n=16$	$n=16$

Preparation of Ag/TiO_2/polymer nanohybrid coatings

As a starting material, standard photocatalyst TiO_2 (Degussa P25, Evonik, Germany) with a specific BET surface area of ~50 m^2/g was used without any treatment. In the first step of the preparation, Ag nanoparticles were placed onto the surface of TiO_2 by photodeposition. In this process TiO_2 powder was dispersed in $AgNO_3$ (Molar, Hungary) solution to obtain Ag-TiO_2, then 2-propanol (Molar, Hungary) was added as a sacrificial donor to promote the photoreduction of Ag^+ ions under UV light illumination by a 300 W Xe-lamp (Hamamtsu L8251, Japan) under 1 h continuous stirring. The prepared Ag-TiO_2 photocatalyst contained 0.5 wt% surface silver nanoparticles. The detailed process of the Ag-TiO_2 synthesis was described in our earlier publications.[18] Dodecyl-sulfate (DS) surfactant molecules were used in 10 wt% to provide hydrophobic character to the photocatalyst particles and increase the dispersibility of the originally hydrophilic photocatalyst particles in the polymer film. The hydrophobically modified TiO_2 and Ag-TiO_2 samples were denoted as DS-TiO_2 and Ag-DS/TiO_2, respectively. During the preparation of the DS-TiO_2 and Ag-DS/TiO_2 photocatalysts the negatively charged surfactant molecules were added to the positively charged TiO_2 suspension at pH = 4.0. The photocatalysts were washed four times then dried and pulverised.

Subsequently, the titanium discs were coated with polyacrylate resin (poly(ethyl acrylate-co-methyl methacrylate; p(EA-co-MMA)) providing the polymer bed for the photocatalyst. The selected photocatalysts were then added to the polymer solution to yield photocatalyst/polymer mass ratios of 60:40. In order to avoid phase separation, 2% polyacrylic acid was added to the dispersion as a chemical stabiliser. The polymer/photocatalyst dispersion was next sonicated for 30 min and sprayed onto the surface of the titanium discs using an AD-318 spray gun (Alder, USA). The resulting film coating was dried to a constant weight (3 ± 0.1 mg/cm^2) at elevated temperature (~120°C). The detailed process of the synthesis was published in our earlier publications.[13] After the preparation of the coating layers the discs were sterilised in a hot air steriliser at 180°C for 45 min. Finally, the discs were subjected to UVC irradiation at 254 nm wavelength for 60 min in order to decompose the upper layers of the polymer bed to uncover the photocatalyst nanoparticles. After cleaning we had five different types of film on the surface of the titanium discs as they are shown in Table 1.

UV-Vis absorption spectroscopy

The determination of the absorption spectra of the composite films was performed with NanoCalc 2000 Micropack spectrophotometer (Ocean Optics, USA) equipped with an integrated sphere and HPX 2000 Mikropack high power xenon lamp. Ocean Optics USB2000 diode array spectrophotometer (USA) was applied for the detection of absorbance.

Scanning electron microscopy

High-resolution secondary electron images were taken with a scanning electron microscope (SEM, Hitachi S4700, Japan) at 500-fold magnification. For the better spatial visualisation of the surface structures the discs were rotated by 45° around their longitudinal (y) axis for image acquisition.

Roughness measurements

Profilometry measurements were performed with Veeco, Dektak 8 Advanced Development Profiler® (Veeco Instruments, USA). The tips had a radius of curvature ~2.5 μm and the force applied to the surface during scanning was ~9.8 μN. The imaging resolution in the x (fast) and y (slow) scan direction was 0.167 μm and 6.35 μm, respectively. The vertical resolution was 40 Å. On each sample, the surface topography of $500 \times 500\ \mu m^2$ area was recorded at six different places and the average roughness values (R_a) were calculated. Measurements were performed before and after the UVC irradiation of the surfaces.

Contact angle measurements

Contact angles were measured to examine the wettability of the surfaces before and after UVC irradiation. The wetting properties of the polymer based reactive composite films were investigated by EasyDrop contact angle measuring system (EasyDrop K-100; Krüss

Gmbh., Germany). The sessile drop method was applied to measure the contact angle. The measurements were carried out at room temperature and the contact angle values were determined before and after UVC irradiation (HPA 400/30 SD type lamp; Philips, Hungary).

Isolation and characterisation of S. salivarius

Clinical isolate of *S. salivarius* was used in this study offered by courtesy of the Institute of Clinical Microbiology, Faculty of Medicine, University of Szeged. The strain was kept at −80°C in Brain Heart Infusion (BHI) broth (Oxoid, UK) containing 12% (v/v) glycerol. The bacteria were cultured for 24 h on Columbia-based agar supplemented with 5% cattle blood (bioMérieux, S.A. Marcy l'Etoile, France) for characterisation and further experiments. The characterisation of the strain was performed with Microflex LT MALDI-TOF mass spectrometer (Bruker Daltonik, Bremen, Germany). Parameter settings were: linear positive ion mode with laser frequency of 60 Hz, mass spectrometry range 2–20 kDa. The sample preparation was performed by formic acid extraction method. Briefly, a single colony was transferred into an Eppendorf tube and suspended by pipetting up and down in 300 µL double-distilled water. Then 900 µL 96% (v/v) ethanol was added and the mixture was suspended again. The mixture was centrifuged for 2 min by 13,000 r/min. The supernatant was removed and the pellet was exsiccated at room temperature. The pellet was re-suspended in the compound of 10 µL 70% aqueous formic acid and 10 µL acetonitrile. After centrifugation 1 µL of the supernatant was pipetted onto the MALDI target plate and 1 µL of MALDI matrix (a solution of 10 mg/ml α-cyano-4-hydroxycinnamic acid in 50% acetonitrile/2.5% trifluoro-acetic acid) was added after drying to the sample at room temperature. The acquired data was automatically analysed by MALDI Biotyper 3.1 software and database (Bruker Daltonik, Bremen, Germany). The species specific identification was performed according to the standard pattern matching approach based on the guidance of the user manual applying log(score) ≥ 2.0.

Investigation of the antibacterial activity of Ag/TiO_2/polymer nanohybrid coatings

S. salivarius was introduced into 0.5 mL reduced BHI broth (Oxoid, Basingstoke, UK) in a density adjusted to McFarland standard 0.5. The bacteria were cultured with

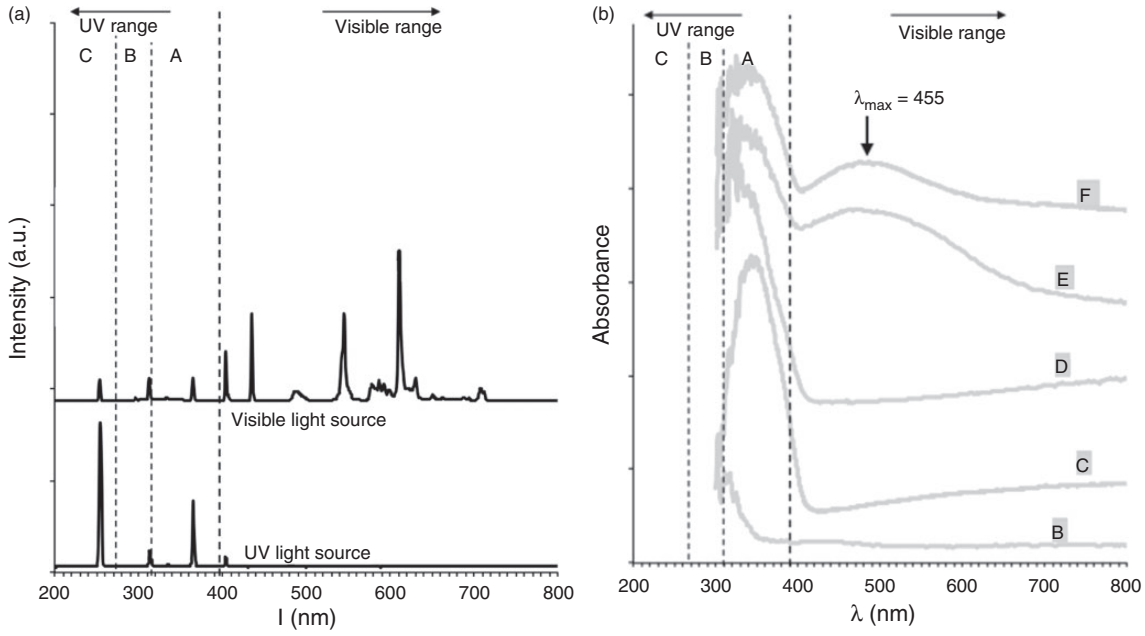

Figure 1. (a) Emission spectra of the UV-Vis light sources. The lower spectrum shows the emission lines of the UV light source that was used for the decomposition of p(EA-co-MMA) copolymer in the last step of the preparation of the samples. The upper spectrum shows the emission lines of both in the UV and VIS ranges of the light source that was used in the microbiology study for irradiation. The low intensity emission lines can be observed at 254, 353 and 393 nm wavelengths. (b) UV-Vis absorption spectra of the experimental groups. The absorption spectra of the C-F experimental groups show large absorption band at ∼ 350 nm wavelength. Another absorption band appears on the absorption spectra of E-F groups in the VIS range between 400 and 550 nm with a maximum of 455 nm.

the coated and control discs in 48-well plates for 4 h under standard conditions at 37°C. The growth of *S. salivarius* on the surface of the discs was measured by means of MTT assay (Sigma Aldrich GmbH, Germany).[19,20]

In order to investigate the photocatalysis mediated antibacterial property of the polymer nanohybrid coatings the experimental groups were divided into 'light' and 'dark' sets. In the 'light' set the discs were irradiated for 10 min at 37°C with UV-Vis light source using a 15 W low-pressure mercury lamp with an intensity of 1.26×10^{-6} E/s in the VIS range (LightTech, Hungary). It has characteristic emission wavelengths mostly above 435 nm. However, it also has emission lines at 254, 353 and 393 nm but the intensity of that lines is significantly lower compared to that of visible range wavelenghts. The emission spectrum of the light source is shown on Figure 1. In the 'dark' or 'control' set the discs were kept in the dark at 37°C. Before irradiation the supernatant was removed from the wells and replaced with 0.2 mL phosphate buffer saline (PBS, PAA, UK) medium. After irradiation 10% 1 mg/mL MTT solution was added to the PBS solution. Following 4 h incubation under standard conditions at 37°C, the medium was gently removed from each well and the crystallised formazan dye was solubilised in absolute isopropanol supplemented with 0.04 M HCl and 10% sodium dodecylsulfate. The optical density of the solution (OD_{540}) was determined at 540 nm with Organon Teknika Reader 530 (Organon Teknika, USA). Four independent experiments were performed including four samples per each experimental group as it is shown in Table 1.

Statistical analyses

Quantitative results of the contact angle (CA, (°)), profile roughness of the surface (R_a (μm)) and absorbance values (MTT, (1)) were analysed.

Data was grouped according to the applied surface treatment and whether the surface was irradiated or not. For data exploration, group means and their 95% confidence intervals were calculated using appropriate t-distributions centered at the sample mean of a given measurement group, with standard deviation equal to the standard error of the measurement within the group and degrees of freedom equal to the sample size in the group less one.

Absorbance values were further analysed to isolate the effects of the different surface treatments and the effect of irradiation on absorbance levels. Comparisons were made within treatment groups between irradiated and dark samples as well as across treatment groups. Due to the large number of comparisons and the highly different variances across groups as seen in Figure 4, a Bayesian multilevel linear model was used for the analysis.[21] The following model was fit to the data in Stan[22] and the output was analysed in Python[23]

$$mtt_i = \alpha_{treatment[i]} + \beta_{treatment[i]} I_i + \epsilon_{treatment[i] \times irradiation[i]}$$

where

- mtt_i is the measured absorbance for the $i = 1 \ldots N$ (198) samples,
- $\alpha_{treatment[i]}$ is the effect of surface treatment of the surface type present on sample i,
- $\beta_{treatment[i]}$ is the effect of irradiation on the surface type of sample i,
- I_i is the indicator variable showing if sample i was irradiated (1) or not (0),
- $\epsilon_{treatment[i]}$ is the error term that is separately approximated for each surface type and irradiation condition.

The parameters were sampled the following way

$$\alpha_{1\ldots K} \sim \text{Normal}(T,\sigma_T) \quad \beta_{1\ldots K} \sim \text{Normal}(C,\sigma_C)$$
$$\epsilon_{1\ldots 2K} \sim Normal\,(0,\sigma_{E=1\ldots 2K})$$

Thus, there are separate treatment, irradiation effects estimated for the $K = 6$ (A-F) surface types and errors with different variances for the $2K = 12$ surface-irradiation combinations. The T (mean MTT absorbance for dark samples), C (mean effect of irradiation), σ_T, σ_C, σ_E scale hyperparameters are estimated from the data along with the $\alpha_{1\ldots K}$, $\beta_{1\ldots K}$ parameters of interest using Markov Chain Monte Carlo (MCMC) sampling in Stan. The hyperparameters were given minimally informative priors to constrain results to sensible ranges and aid sampler convergence. Sensitivity analysis was done to confirm priors.

The result of interest of the MCMC sampling is an empirical joint posterior distribution for the $\alpha_{1\ldots K}$, $\beta_{1\ldots K}$ parameters (mean surface treatment and irradiation effects), which allows direct comparison of the means as well as the actual measurements expected from future experiments. The probability distributions of the contrasts of the means as well as the predictive differences between individual measurements (containing data level variation) were calculated between and across treatment groups and irradiation conditions and were summarised by the 95% equal tailed probability intervals and expected values of the distributions. These results are close to the values given by the t-distributions used in the data exploration; however, they are not necessarily equal due to the difference in the interpretation of a Bayesian credible interval and classical confidence intervals.

We used the joint posterior distributions of the parameters to simulate comparisons of absorbance for individual samples and superimposed the resulting 95% CIs on the group means to indicate data level uncertainty. Data tables and plots were prepared using R.[24]

Results

The coating of the titanium discs by photocatalyst containing polymer changes the optical properties of the surfaces as it is shown on the absorbance spectra (Figure 1). As the result of silver coating, an absorption band appeared on the spectrum between 400 and 600 nm (visible range) with a maximum at 455 nm.

The SEM images revealed significant differences in the morphology of the intact and coated TiO_2 surfaces at 500-fold magnification (Figure 2). Figure 2(a) shows a sandblasted and acid etched TiO_2 surface that represents the typical surface pattern of a conventional titanium dental implant. Figure 2(b) shows a smooth surface that is obtained after acrylate-based copolymer film coating of the acid etched and sandblasted TiO_2 surface. Figure 2(c) and (d) shows the amorphous surface pattern in the micrometre range when the titanium discs were coated with a TiO_2 photocatalyst containing copolymer film; whereas characteristic rounded grains appeared on the surfaces of the discs that were coated with the silver photocatalyst containing copolymer film (Figure 2(e) and (f)).

The quantitative measurement of roughness (R_a (μm)) on the surface of the discs by profilometry provided results that confirmed the differences in the surface pattern of the samples that were observed on the representative SEM images (Figure 3). There was considerable

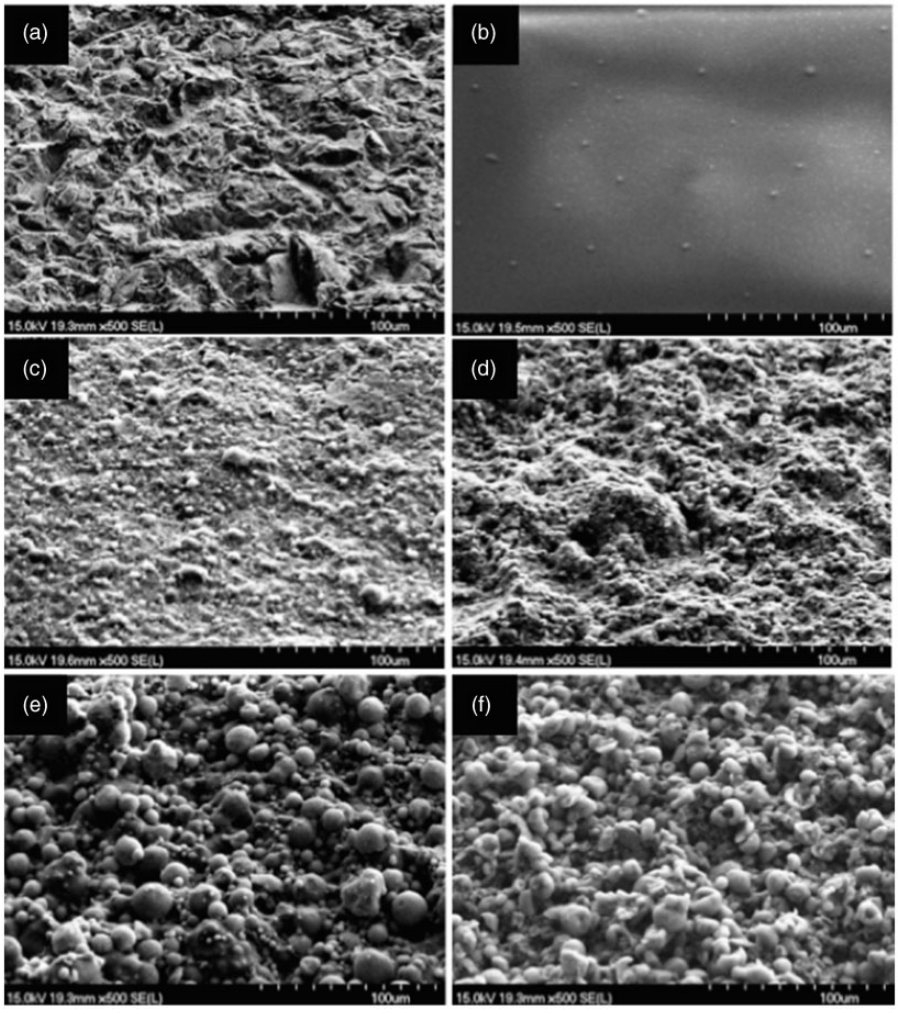

Figure 2. Representative SEM images of the experimental groups. (a) Sandblasted and acid etched surface (Group A), (b) p(EA-co-MMA) copolymer (Group B), (c) 60 wt% TiO_2: 40 wt% copolymer (Group C), (d) 60 wt% DS-TiO_2: 40 wt% copolymer (Group D), (e) 60 wt% Ag-TiO_2: 40 wt% copolymer (Group E), (f) 60 wt% Ag-DS/TiO_2: 40 wt% copolymer (Group F).

variation in the roughness values of the different surfaces; however, no significant difference could be observed between untreated and UVC-treated samples within the same surface treatments (upper panel of Figure 4).

Before UVC irradiation contact angle (CA, (°)) measurements showed that the (A), (C), (D) and (F) surfaces were hydrophilic (CA $\leq 90°$), while (B) and (E) were hydrophobic. Photocatalyst containing surfaces (C, D, E and F) became superhydrophilic after UVC (254 nm) irradiation, while the polymer coated (B) remained hydrophobic. The mean contact angles for each treatment group and irradiation condition and their 95% CIs can be seen on the centre panel of Figure 4.

Concerning the characterisation of the clinical isolate of bacterium strain, the MALDI-TOF MS gave a species level identification with log(score) = 2.184 for *S. salivarius* strain.

Absorbance levels (MTT^1) had distinct group means across most treatment and irradiation conditions as suggested by the minimal overlap in the confidence intervals (lower panel of Figure 4). The linear decomposition of the absorbance levels into surface effects, surface based irradiation effects and noise yielded comparative results. Under dark conditions, the group means of absorbance in the TiO_2 photocatalyst containing (C) and (D) experimental groups was higher than those of the Ag/TiO_2/polymer nanohybrid films in the (E) and (F) groups. This suggests that more *S. salivarius* attached to the surface of TiO_2 containing polymer films than to Ag/TiO_2/polymer nanohybrid films. The mean absorbance in the (E) and (F) groups was credibly lower than in any of the other groups. The control (A) group had the highest mean absorbance of all groups, being credibly higher than (B) and (D), but compared to group (C) a zero difference still falls in the 95% credible interval.

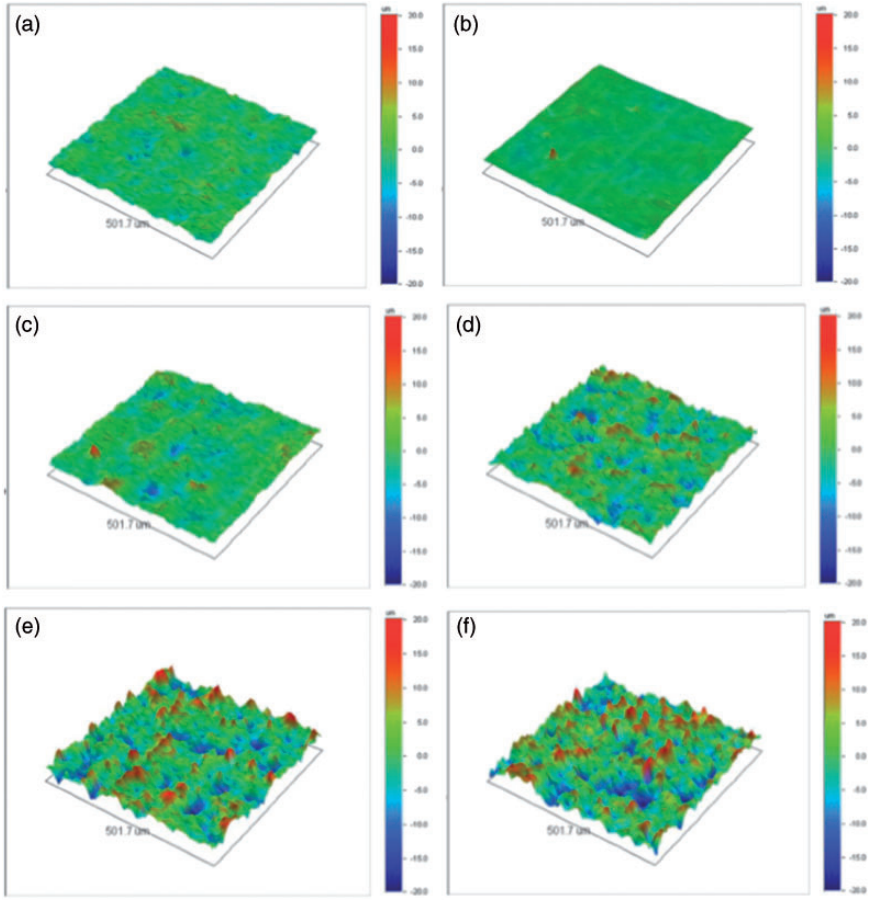

Figure 3. Three-dimensional roughness profiles of the surfaces. The average roughness values of the surfaces are the following: (a) $R_{a,A} = 1.85$ μm for sandblasted and acid etched surface (Group A), (b) $R_{a,B} = 1.19$ μm for p(EA-co-MMA) copolymer (Group B), (c) $R_{a,C} = 2.33$ μm for 60 wt% TiO_2: 40 wt% copolymer (Group C), (d) $R_{a,D} = 3.70$ μm for 60 wt% DS TiO_2: 40 wt% copolymer (Group D), (e) $R_{a,E} = 5.17$ μm for 60 wt% Ag-TiO_2: 40 wt% copolymer (Group E), (f) $R_{a,F} = 5.60$ μm for 60 wt% Ag-DS/TiO_2: 40 wt% copolymer (Group F).

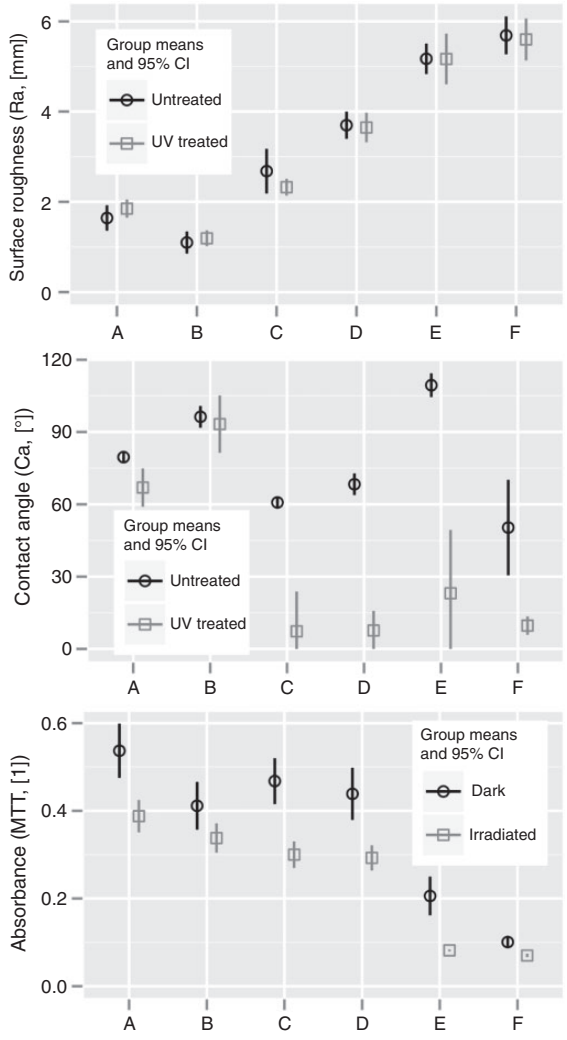

Figure 4. Means and 95% CIs of surface roughness, contact angles and absorbance across surface types and irradiation conditions. There was considerable variation in surface roughness between the different surfaces; however, no significant difference could be observed between untreated and UVC-treated samples within the same surface treatments (top panel). Before UVC treatment contact angle (CA (°)) measurements showed that the (A), (C), (D) and (F) surfaces were hydrophilic, while (B) and (E) were hydrophobic. Photocatalyst containing surfaces (C, D, E and F) became superhydrophilic after UVC (254 nm) treatment, while the polymer coated (B) remained hydrophobic. The mean contact angles for each treatment group before and after UVC treatment and their 95% CIs can be seen on the centre panel. On the bottom panel the mean MTT absorbance values are shown before and after UV-Vis irradiation. The lack of overlap suggests significant differences between certain groups; however, due to the apparent differences in variances, a Bayesian analysis was used to confirm this.

The net effect of UV-Vis irradiation on absorbance values was negative in each group (95% CI excluded zero), indicating that the viability of bacteria was reduced on the irradiated surfaces. The same tendency was observed on the control surface (A) after irradiation than in C, D and E, F experimental groups. However, this reduction was the lowest in the (B) experimental group where the control surface was coated with p(EA-co-MMA) polymer without any photocatalyst content. In absolute magnitude the highest irradiation effect of -0.15 $CI_{95\%}(0.09, 0.21)$ was observed in the (C) group, while relative to the dark levels the (E) group showed the largest percentage change of 60% $CI_{95\%}$ (50%, 67%), followed by group (C) 33% $CI_{95\%}$ (23%, 42%). The credible differences are listed in Tables 2 to 4 across comparisons both in the group means and the individual measurements, as well as an estimation of the percentage of the samples that we expect to have lower/higher absorbance in the comparison.

Discussion

Our results show that the photocatalytic content of the copolymer films significantly affects the antibacterial activity of their surface in in vitro experimental setting. The TiO_2 photocatalyst containing copolymer films show less intense antibacterial effect without irradiation than the coupled Ag/TiO_2 containing films; however, the irradiation triggered similar drops in the absorbance level suggesting the photocatalytic decomposition of bacteria in each experimental group. On the other hand, the influence of physical parameters of the surfaces on the contamination level, such as microroughness and hydrophilic property of the copolymer films could not be credibly determined in this experimental setting.

The applied light source for irradiation in the microbiology study had emission lines mainly in the VIS range (above 435 nm) that cannot explain the universal drop of the absorbance levels in each experimental group (Figure 5). An absorption band appeared on the UV-Vis absorption spectra of E and F groups between 400 and 550 nm with a maximum of 455 nm indicating the plasmonic effect of silver nanoparticles, which enhances the photocatalytic efficiency of silver doped TiO_2 under visible light. This enhanced photocatalytic efficiency might contribute to the absorbance drop in the E and F experimental groups but not in the C-D and the A-B groups. Concerning pure TiO_2, the band gap is 3.2 eV for anatase and 3.0 eV for rutile (two polymorphs of TiO_2), which means that UV light ($\lambda \leq 387$ nm) is required to excite an electron from the valance band to the conduction band in photocatalysis.[25] Hence, the absorbance drop in C-D and A groups might be triggered by the low-intensity emission in the UV range (353 nm and 393 nm) of the light source that was used for the irradiation of the contaminated samples in the microbiology study (Figure 1). The higher absorbance drop in C and D groups compared to

Table 2. Credible intervals for the difference in absorbance levels of the dark and UV-Vis irradiated experimental groups within the same surface types. A black typeface is used where the credible interval excludes zero, bold where the interval overlaps zero. Intervals for the mean difference and also for individual differences are given, as well as an estimation of the percent of the samples that will have lower/higher absorbance in a one-to-one comparison.

	95% CI for mean difference in MTT absorbance			95% CI for individual differences in absorbance			Predicted % of diffs. being positive/negative	
Comparison	Low	Mean	High	Low	Mean	High	(+)	(−)
Ad – Al	0.07	0.13	0.20	**−0.18**	**0.13**	**0.44**	81	19
Bd – Bl	0.02	0.08	0.14	**−0.19**	**0.08**	**0.36**	73	27
Cd – Cl	0.09	0.15	0.21	**−0.12**	**0.15**	**0.41**	87	13
Dd – Dl	0.08	0.13	0.19	**−0.15**	**0.13**	**0.42**	83	17
Ed – El	0.08	0.12	0.17	**−0.07**	**0.12**	**0.31**	90	10
Fd – Fl	0.02	0.03	0.04	**−0.02**	**0.03**	**0.08**	89	11

Table 3. Credible intervals for the difference in absorbance levels of each surface type when kept in the dark. A black typeface is used where the credible interval excludes zero, bold where the interval overlaps zero. Intervals for the mean difference and also for individual differences are given, as well as an estimation of the percent of the samples that will have lower/higher absorbance in a one-to-one comparison.

	95% CI for mean difference in MTT absorbance			95% CI for individual differences in absorbance			Predicted % of diffs. being positive/negative	
Comparison	Low	Mean	High	Low	Mean	High	(+)	(−)
Ad – Bd	0.03	0.11	0.18	**−0.25**	**0.11**	**0.46**	73	27
Ad – Cd	**−0.01**	**0.07**	**0.15**	**−0.28**	**0.07**	**0.43**	66	34
Ad – Dd	0.02	0.10	0.17	**−0.28**	**0.10**	**0.47**	70	30
Ad – Ed	0.25	0.32	0.39	**−0.01**	**0.32**	**0.65**	97	3
Ad – Fd	0.36	0.42	0.48	0.14	0.42	0.70	100	0
Bd – Cd	**−0.11**	**−0.04**	**0.03**	**−0.36**	**−0.04**	**0.29**	41	59
Bd – Dd	**−0.08**	**−0.01**	**0.06**	**−0.36**	**−0.01**	**0.34**	47	53
Bd – Ed	0.15	0.21	0.28	**−0.09**	**0.21**	**0.52**	92	8
Bd – Fd	0.26	0.32	0.37	0.07	0.31	0.56	99	1
Cd – Dd	**−0.05**	**0.03**	**0.10**	**−0.32**	**0.03**	**0.37**	56	44
Cd – Ed	0.18	0.25	0.31	**−0.05**	**0.25**	**0.55**	95	5
Cd – Fd	0.30	0.35	0.40	0.11	0.35	0.59	100	0
Dd – Ed	0.16	0.22	0.29	**−0.10**	**0.22**	**0.54**	92	8
Dd – Fd	0.27	0.33	0.38	0.06	0.33	0.59	99	1
Ed – Fd	0.06	0.10	0.15	**−0.10**	**0.10**	**0.30**	85	15

control group A might be explained by the differences in the electron structure of the sandblasted/acid etched bulk TiO_2 surface and the nanocrystalline TiO_2. In C and D groups the nanocrystalline TiO_2 photocatalyst contains a combination of anatase (~80%) and rutile (~20%).[16] The conduction band potential of rutile is more positive than that of anatase, which means that the rutile phase may act as an electron sink for photo-generated electrons from the conduction band of the anatase phase, therefore it reduces the recombination rate of charge carriers. When recombination occurs the excited electron reverts to the valance band without reacting with the adsorbed species.[26] Recombination might take place at a higher rate in the electron structure of the sandblasted/acid-etched TiO_2 (group A) than in the nanocrystalline (Degussa P25) photocatalyst (groups C-D) that may explain the lower effect of irradiation in group A. Concerning the absorbance drop in group B, the low-intensity UVC light may be sufficient to decompose the uppermost layer of the

Table 4. Credible intervals for the difference in absorbance levels of each surface type after UV-Vis irradiation. A black typeface is used where the credible interval excludes zero, bold where the interval overlaps zero. Intervals for the mean difference and also for individual differences are given, as well as an estimation of the percent of the samples that will have lower/higher absorbance in a one-to-one comparison.

	95% CI for mean difference in MTT absorbance			95% CI for individual differences in absorbance			Predicted % of diffs. being positive/negative	
Comparison	Low	Mean	High	Low	Mean	High	(+)	(−)
AI – BI	0.01	006	0.10	**−0.16**	**0.06**	**0,27**	70	30
AI – CI	0.04	0.09	0.14	**−0.12**	**0.09**	**0,29**	81	19
AI – DI	0.05	0.10	0.14	**−0.10**	**0.10**	**0.30**	84	16
AI – EI	0.27	0.31	0.35	0.15	0.31	0.47	100	0
AI – FI	0.29	0.32	0.36	0.16	0.32	0.48	100	0
BI – CI	**−0.01**	**0.03**	**0.08**	**−0.16**	**0.03**	**0.23**	63	37
BI – DI	**0.00**	**0.04**	**0.08**	**−0.15**	**0.04**	**0.23**	68	32
BI – EI	0.22	0.25	0.29	0.11	0.25	0.40	100	0
BI – FI	0.23	0.27	0.30	0.12	0.27	0.41	100	0
CI – DI	**−0.03**	**0.01**	**0.05**	**−0.17**	**0.01**	**0.19**	54	46
CI – EI	0.19	0.22	0.25	0.09	0.22	0.35	100	0
CI – FI	0.20	0.23	0.27	0.10	0.23	0.37	100	0
DI – EI	0.18	0.21	0.24	0.09	0.21	0.34	100	0
DI – FI	0.20	0.22	0.25	0.10	0.22	0.35	100	0
EI – FI	0.01	0.01	**0.02**	**−0.01**	**0.01**	**0.03**	88	12

copolymer film that might entail the detachment of the bacteria from the surface.

Sandblasting and acid etching – or their combination – are the most common applied surface treatment methods to improve the biocompatibility of titanium dental implants with bone tissue, thus such surfaces are often used as reference in in vitro biocompatibility and microbiology studies.[27,28] The major limitation of the sandblasted and acid etched surfaces is that they are prone to infection because of their microrough ($R_a > 200$ nm) surface that favors the attachment of pathogenic bacteria.[29,30] On the other hand, we found that the absorbance was decreasing with the higher surface roughness, however we did not attempt to confirm these relations between the R_a and absorbance values in our experimental setting (Figure 4). Concerning the wettability of the films, the visual inspection of the trends across sample did not indicate any correspondence between the hydrophilic/hydrophobic character of the films and the ability of *S. salivarius* to colonise the surfaces (Figure 4).

Contrarily, we found that the photocatalytic content of the copolymers significantly influenced the antibacterial activity of the coating films. In groups A-D, markedly higher initial absorbance values were measured before irradiation than in E-F groups where silver was present (Figure 5). This finding is in line with the innate antibacterial activity of silver coated surfaces that has already been widely demonstrated by other research groups.[31,32] However, our results show that the TiO_2 photocatalyst containing copolymer films may also exhibit considerable photo-induced antibacterial activities.

It is also important to note, that the analysis of finite population variances of the treatment effects (chemical composition of coating films), irradiation effects and noise terms across the sample indicated that noise still plays a large role in determining the absorbance of individual samples.[21] The standard deviation from the grand mean absorbance due to different surface treatments is 0.15, while both irradiation effects and noise has standard deviations of 0.08. The latter is also the central value of highly different standard deviations across sample groups. Therefore, the results of the above paragraphs hold for the means of several measurements and may hold for a subset of the comparisons for individual samples. Most notably, when comparing one irradiated sample to a dark sample of the same surface type, it is difficult to predict which one will have a lower absorbance since irradiation effects and noise are of the same magnitude. For example, in spite we are 95% certain that a group of irradiated (D) samples on average have lower absorbances than a similar groups of dark (D) samples, we only expect approximately 83% of the actual samples to behave this way, due to the variation between individual measurements

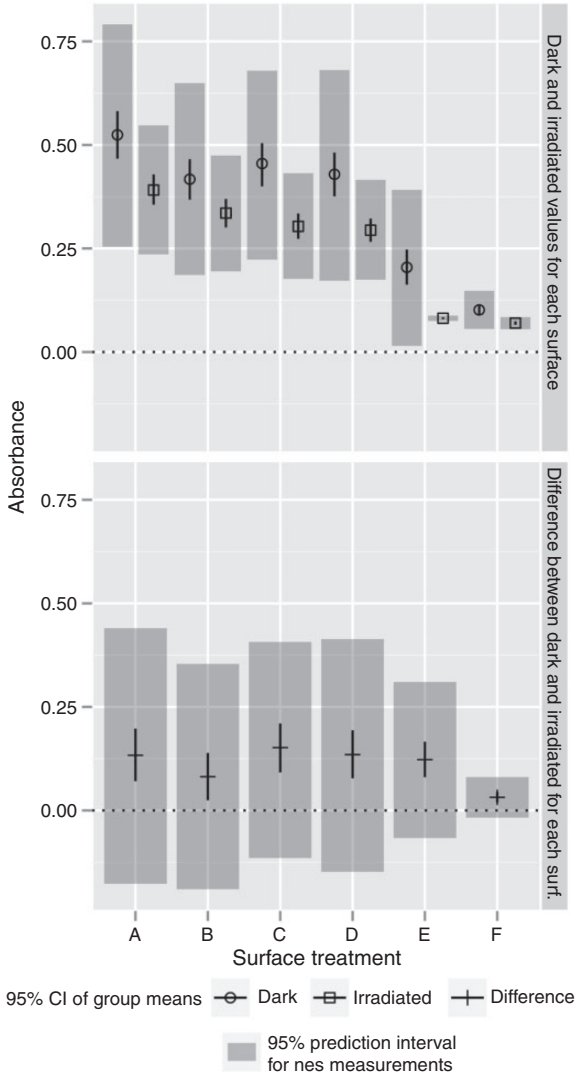

Figure 5. Credible intervals of absorbance across surface types and irradiation conditions and credible differences between irradiated and dark samples within the same surface types. 95% CIs of group means and individual measurements displayed. Under dark conditions, the group means of absorbance in the TiO_2 photocatalyst containing (C) and (D) experimental groups was higher than those of the coupled Ag/TiO_2 containing films in the (E) and (F) groups. The mean absorbance in the (E) and (F) groups was credibly lower than in any of the other groups. The control (A) group had the highest mean absorbance of all groups, being credibly higher than (B) and (D), but compared to group (C) a zero difference still falls in the 95% credible interval.

within the groups. This is in accordance with our observations, where some measurements of the irradiated samples had higher absorbance than their dark counterparts with the same surface, while on average irradiated samples always had lower values.

Our findings suggest that the research of the TiO_2 containing photocatalytic copolymers and their application as coating materials on the surface of dental implants might be a promising subject area in the field of biomaterials. Photocatalytic coatings may provide a novel approach for the less invasive decontamination of infected dental implants via enhanced photo-induced release of reactive oxidative species.[33] In contrast to mechanical decontamination, the potential benefit of such surfaces might be that photocatalysis induced decontamination may preserve the integrity of the biologically active micro- and nanostructures on the surface, which is essential to support the bone healing and osseointegration of the implant.[34] The current obstacle of such approach is that the early diagnosis of peri-implantitis is often very difficult because of the limitations of radiographic examinations and the absence of mobility compared to natural teeth. Thus, when it comes to surgical decontamination, the surface of the implant is often covered by a thick biofilm that may limit the penetration of the light that is to reach the surface to induce photocatalytic decontamination. Therefore, further research and development is needed to improve the photocatalytic antibacterial activity of biocompatible coatings, however it should also be accompanied by the development of less invasive surgical debridement techniques that can secure the integrity of such surfaces. The titration of silver content may be a good approach to find a balance between enhanced photocatalytic activity and biocompatibility of copolymer-based coating films. Dental curing units with LED and plasma arc light sources are widely used in dental practices, have emission both in the ultraviolet and visible light (blue) ranges, therefore could be used for the induction of photocatalytic decomposition of biofilms on photosensitised copolymers.[35]

Acknowledgments

The authors express their gratitude to G Terhes and E Urbán (Institute of Clinical Microbiology, Faculty of Medicine, University of Szeged) for providing *S. salivarius*. The authors also thank to K Buzás (Laboratory of Tumor Immunology and Pharmacology, Institute of Biochemistry, Biological Research Center, Hungarian Academy of Sciences) for the valuable discussions on the microbiological experimental setup. Special acknowledgments to Denti System Kft for supplying our research group with commercially pure titanium for the experiments. The authors are grateful to M Weszl (NanoTi Limited, Birmingham) for the helpful advice on the concept of the paper, interpretation of the results, critical reviewing and rephrasing of the article.

Declaration of Conflicting Interests

The author(s) declared no potential conflicts of interest with respect to the research, authorship, and/or publication of this article.

Funding

The author(s) disclosed receipt of the following financial support for the research, authorship, and/or publication of this

article: The present study was supported by the following grants: TÁMOP-4.2.1/B-09/1/KONV-2010-0005—Creating the Centre of Excellence at the University of Szeged, TÁMOP-4.2.2.A-11/1/KONV–2012-0047—Biological and environmental responses initiated by new functional materials projects supported by the European Union and co-financed by the European Regional Development Fund, Hungarian-French Intergovernmental S&T Cooperation Programme TéT_10-1-2011-0708. K Turzó was supported by the János Bolyai Research Scholarship of the Hungarian Academy of Sciences.

References

1. Heuer W, Stiesch M and Abraham WR. Microbial diversity of supra- and subgingival biofilms on freshly colonized titanium implant abutments in the human mouth. *Eur J Clin Microbiol Infect Dis* 2010; 30: 193–200.
2. Charalampakis G, Leonhardt Å, Rabe P, et al. Clinical and microbiological characteristics of peri-implantitis cases: A retrospective multicentre study. *Clin Oral Implants Res* 2012; 23: 1045–1054.
3. Atieh MA, Alsabeeha NHM, Faggion CM, et al. The frequency of peri-implant diseases: A systematic review and meta-analysis. *J Periodontol* 2013; 84: 1586–1598.
4. Norowski PA Jr and Bumgardner JD. Biomaterial and antibiotic strategies for peri-implantitis: A review. *J Biomed Mater Res Part B: Appl Biomater* 2009; 88: 530–543.
5. Rams TE, Degener JE and van Winkelhoff AJ. Antibiotic resistance in human peri-implantitis microbiota. *Clin Oral Implants Res* 2014; 25: 82–90.
6. Prathapachandran J and Suresh N. Management of peri-implantitis. *Dental Res J* 2012; 9: 516–521.
7. Gallo J, Holinka M and Moucha CS. Antibacterial surface treatment for orthopaedic implants. *Int J Mol Sci* 2014; 15: 13849–13880.
8. Hasan J, Crawford RJ and Ivanova EP. Antibacterial surfaces: The quest for a new generation of biomaterials. *Trends Biotechnol* 2013; 31: 295–304.
9. De Giglio E, Cafagna D, Cometa S, et al. An innovative, easily fabricated, silver nanoparticle-based titanium implant coating: Development and analytical characterization. *Anal Bioanal Chem* 2013; 405: 805–816.
10. Kruszewski M, Brzoska K, Brunborg G, et al. Toxicity of silver nanomaterials in higher eukaryotes. In: Fishbein JC (ed.) *Advances in molecular toxicology*. New York: Elsevier, 2011, pp. 179–218.
11. Xiong Z, Ma J, Ng WJ, et al. Silver-modified mesoporous TiO2 photocatalyst for water purification. *Water Res* 2011; 45: 2095–2103.
12. Veres A, Rica T, Janovak L, et al. Silver and gold modified plasmonic TiO2 hybrid films for photocatalytic decomposition of ethanol under visible light. *Catal Today* 2012; 181: 156–162.
13. Veres A, Janovak L, Bujdoso T, et al. Silver and phosphate functionalized reactive TiO_2/polymer composite films for destructions of resistant bacteria using visible light. *J Adv Oxid Technol* 2012; 15: 205–216.
14. Su C, Tseng CM, Chen LF, et al. Sol–hydrothermal preparation and photocatalysis of titanium dioxide. *Thin Solid Films* 2006; 498: 259–265.
15. Linsebigler AL, Lu G and Yates JT. Photocatalysis on TiO2 surfaces: Principles, mechanisms, and selected results. *Chem Rev* 1995; 95: 735–758.
16. Pelaez M, Nolan N, Pillai S, et al. A review on the visible light active titanium dioxide photocatalysts for environmental applications. *Appl Catal B: Environ* 2012; 125: 331–349.
17. Pita PPC, Rodrigues JA, Ota-Tsuzuki C, et al. Oral streptococci biofilm formation on different implant surface topographies. *BioMed Res Int* 2015; 2015: 159625.
18. Veres A, Menesi J, Juhasz A, et al. Photocatalytic performance of silver-modified TiO_2 embedded in poly (ethyl-acrylate-co-methyl metacrylate) matrix. *Colloid Polym Sci* 2014; 292: 207–217.
19. Ionescu A, Wutscher E, Brambilla E, et al. Influence of surface properties of resin-based composites on in vitro Streptococcus mutans biofilm development. *Eur J Oral Sci* 2012; 120: 458–465.
20. Mosmann T. Rapid colorimetric assay for cellular growth and survival: Application to proliferation and cytotoxicity assays. *J Immunol Meth* 1983; 65: 55–63.
21. Gelman A and Hill J. *Data analysis using regression and multilevel/hierarchical models*. Cambridge: Cambridge University Press, 2007.
22. Stan: A C++Library for Probability and Sampling, Version 2.7.0., 2015.
23. Python Software Foundation. Python language reference, version 2.7.8, 2015.
24. R Core Team. R: A language and environment for statistical computing, version 3.2.1. R Foundation for Statistical Computing, Vienna, Austria, 2015.
25. Chandiran AK, Abdi-Jalebi M, Nazeeruddin MK, et al. Analysis of electron transfer properties of ZnO and TiO_2 photoanodes for dye-sensitized solar cells. *ACS Nano* 2014; 8: 2261–2268.
26. Liqiang J, Yichun Q, Baiqi W, et al. Review of photoluminescence performance of nano-sized semiconductor materials and its relationships with photocatalytic activity. *Solar Energy Mater Solar Cells* 2006; 90: 1773–1787.
27. Hirano T, Sasaki H, Honma S, et al. Proliferation and osteogenic differentiation of human mesenchymal stem cells on zirconia and titanium with different surface topography. *Dental Mater J* 2015; 34: 872–880.
28. Meng W, Zhou Y, Zhang Y, et al. Effects of hierarchical micro/nano-textured titanium surface features on osteoblast-specific gene expression. *Implant Dent* 2013; 22: 656–661.
29. Teughels W, Van Assche N, Sliepen I, et al. Effect of material characteristics and/or surface topography on biofilm development. *Clinical Oral Implants Res* 2006; 17: 68–81.
30. Lee A and Wang HL. Biofilm related to dental implants. *Implant Dent* 2010; 19: 387–393.
31. Tilmaciu CM, Mathieu M, Lavigne JP, et al. In vitro and in vivo characterization of antibacterial activity and biocompatibility: A study on silver-containing phosphonate monolayers on titanium. *Acta Biomater* 2015; 15: 266–277.
32. Massa MA, Covarrubias C, Bittner M, et al. Synthesis of new antibacterial composite coating for titanium based

on highly ordered nanoporous silica and silver nanoparticles. *Mater Sci Eng C* 2014; 45: 146–153.
33. de Melo WCMA, Avci P, de Oliveira MN, et al. Photodynamic inactivation of biofilm: Taking a lightly colored approach to stubborn infection. *Expert Rev Anti-Infect Ther* 2013; 11: 669–693.
34. Wheelis SE, Gindri IM, Valderrama P, et al. Effects of decontamination solutions on the surface of titanium: Investigation of surface morphology, composition, and roughness. *Clin Oral Implants Res* 2015.
35. Tallosy SP, Janovak L, Menesi J, et al. LED-light activated antibacterial surfaces using silver-modified TiO_2 embedded in polymer matrix. *J Adv Oxid Technol* 2014; 17: 9–16.